Biomaterials 34 (2013) 9754–9762

Contents lists available at ScienceDirect

Biomaterials

journal homepage: www.elsevier.com/locate/biomaterials

Relationships among cell morphology, intrinsic cell stiffness and cell–substrate interactions

Martin Y.M. Chiang [a, *, 1], Yanzi Yangben [b, 1], Nancy J. Lin [a, 1], Julia L. Zhong [b, 1], Li Yang [b, *, 1]

[a] Biosystems and Biomaterials Division, National Institute of Standards and Technology (NIST), Gaithersburg, MD 20899, USA[2]
[b] College of Bioengineering, Chongqing University, Chongqing, China

ARTICLE INFO

Article history:
Received 8 August 2013
Accepted 4 September 2013
Available online 26 September 2013

Keywords:
Cell modulus
Cell morphology
Substrate rigidity
Roundness
Cell–material interaction
Free energy

ABSTRACT

Cell modulus (stiffness) is a critical cell property that is important in normal cell functions and increasingly associated with disease states, yet most methods to characterize modulus may skew results. Here we show strong evidence indicating that the fundamental nature of free energies associated with cell/substrate interactions regulates adherent cell morphology and can be used to deduce cell modulus. These results are based on a mathematical model of biophysics and confirmed by the measured morphology of normal and cancerous liver cells adhered on a substrate. Cells select their final morphology by minimizing the total free energy in the cell/substrate system. The key mechanism by which substrate stiffness influences cell morphology is the energy tradeoff between the stabilizing influence of the cell-substrate interfacial adhesive energy and the destabilizing influence of the total elastic energies in the system. Using these findings, we establish a noninvasive methodology to determine the intrinsic modulus of cells by observing global changes in cell morphology in response to substrate stiffness. We also highlight the importance of selecting a relevant morphological index, cell roundness, that reflects the interchange between forms of energy governing cell morphology. Thus, cell-substrate interactions can be rationalized by the underlying biophysics, and cell modulus is easily measured.

Published by Elsevier Ltd.

1. Introduction

The impact of cell modulus (the deformability of cells or resistance to morphological change) extends beyond knowledge of a mechanical property to include cellular processes important in developmental biology, pathology, molecular biology, etc., as well as cell–material interactions in tissue engineering and regenerative medicine. For instance, cell modulus also affects many cell functions [1–3], correlates with disease states [4,5], has potential as a biomarker to distinguish normal and cancerous cells, and corresponds with embryonic stem cell fate [6,7]. Smooth muscle cell stiffness has been recognized recently to contribute to aortic stiffening, which relates to a host of aging processes and vascular diseases, including hypertension, atherosclerosis, and aortic aneurysms [8]. Glial cell stiffness has also been suggested as both a mechanism responsible for rigid glial scars that impair neuroregeneration after spinal cord injury as well as a target for regeneration therapies [9]. Likewise, tumor cell modulus corresponds with metastatic potential, and biochemical means to alter the modulus can change that metastatic potential [10], leading to the proposal of cell modulus as a “mechanical signature” of cancer cells and potentially a new biomarker of malignancy to aid in diagnosis and treatment of cancer [11]. In addition, controlling cell modulus is one potential approach to direct stem cells into the desired lineage for regenerative medicine applications, where a key challenge is optimizing mechanical and structural properties of scaffolds (substrates) to promote the desired tissue regeneration [12].

Our objective is to provide a noninvasive measurement of intrinsic cell modulus based on fundamental free energy concepts in cell-substrate interactions. Currently available methods to measure cell modulus typically involve either physical perturbation of cells adherent to two-dimensional substrates [11,13,14], where mechanical contributions from the substrate can be difficult to delineate from cell properties (*e.g.*, atomic force

* Corresponding authors.
E-mail addresses: martin.chiang@nist.gov (M.Y.M. Chiang), yangli@cqu.edu.cn (L. Yang).
[1] Authors contributed equally in this work.
[2] Official contribution of the National Institute of Standards and Technology; not subject to copyright in the United States.

0142-9612/$ – see front matter Published by Elsevier Ltd.
http://dx.doi.org/10.1016/j.biomaterials.2013.09.014

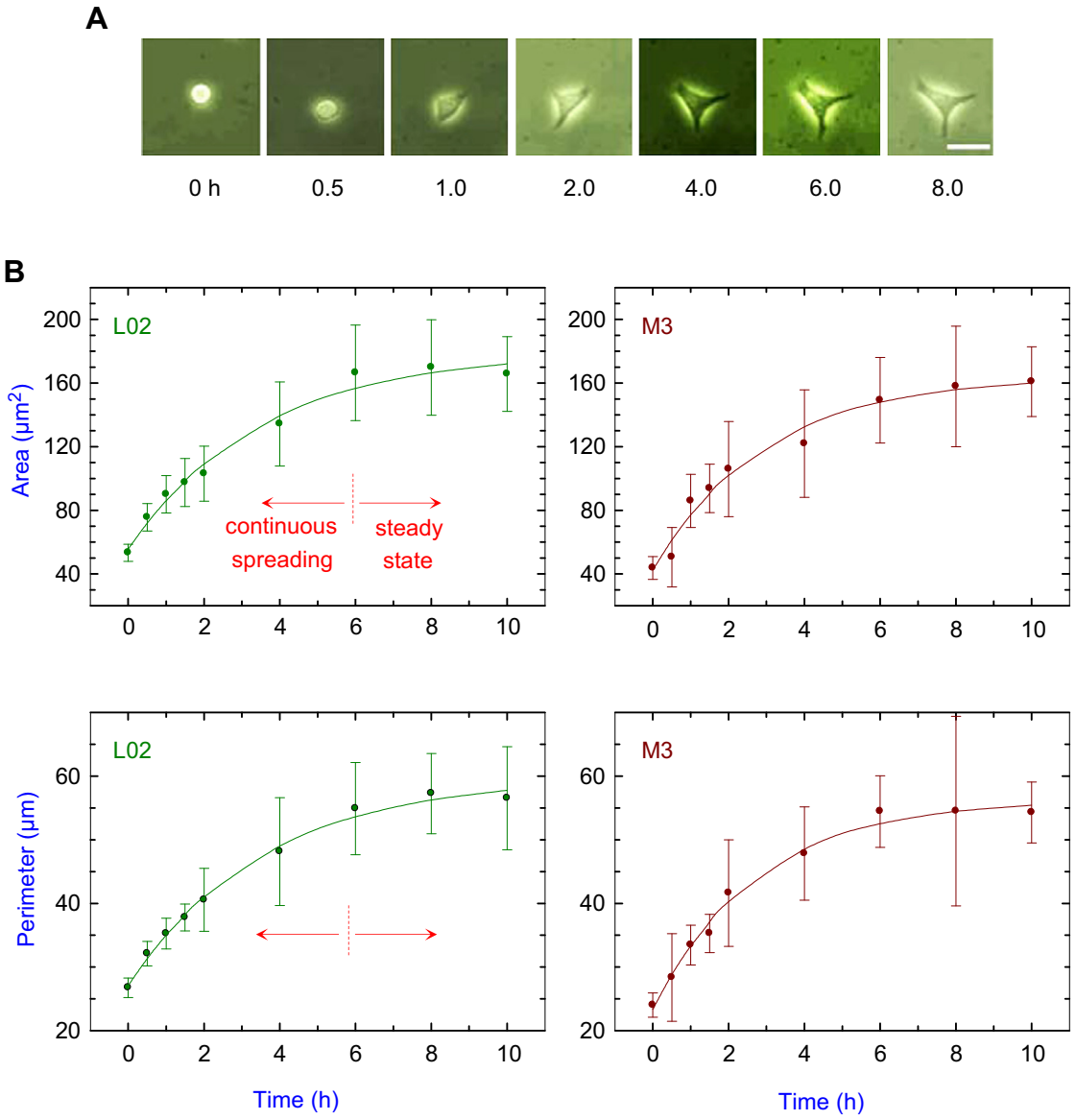

Fig. 1. The process of cell spreading. A, Typical microphotographs of M3 cell spreading obtained at different time points up to 10 h. Scale = 20 μm. B, Cell area and perimeter obtained as a function of time for normal (L02) and cancerous (M3) liver cells attached to glass substrates coated with fibronectin (2.5 μg/mL). In general, cell spreading exhibits three regimes (three-phases) starting with an initial basal growth regime for the nucleation of adhesion sites (not recorded for the plots). This basal phase is followed by a phase of fast continuous spreading, a non-steady process where cells constantly move and modulate their shapes. Finally, cell spreading slows down and effectively reaches a steady state. Cells were imaged for 10 h using inverted phase contrast microscopy. Each data point represents the mean value from at least 30 cells, and each error bar is one standard deviation and represents the standard uncertainty. Lines are drawn to aid the reader's eyes.

microscopy (AFM), poking, magnetic twisting cytometry, micropipette aspiration), or qualitative evaluation of deformability via filtration processes [15]. These measurements provide a relative or apparent cell modulus that depends on the measurement technique rather than an intrinsic modulus, which is a fundamental property of the cell that is independent of cell adhesion and assembled cytoskeletal networks of adherent cells. Our interest here is not to compare the relative merits of existing methods but to establish a method to quantify intrinsic cell modulus based on cell-substrate interactions. The effect of deformable substrates on cells is an active research area in cell mechanics [16–20]. *In vitro* studies of cells on substrates with different moduli indicate that cells sense substrate modulus and respond by changing their cell morphology (shape and size) [14,21]. This morphological change is accomplished through assembly/disassembly of focal adhesions and used by cells to regulate physiological processes [22–25]. In this investigation, we show that the underlying physics of free energy in the cell/substrate system can describe how substrate modulus is translated into cell morphology, and that morphological stability of cells is dictated by the minimum total free energy in the system provided that the surrounding chemical environment remains constant. The combination of mathematical modeling and cell measurements reveals a new method to obtain intrinsic cell modulus using the variation of cell morphology in response to substrate stiffness. Moduli of normal and cancerous cells are quantified via our morphology analysis and compared with conventional AFM measurements.

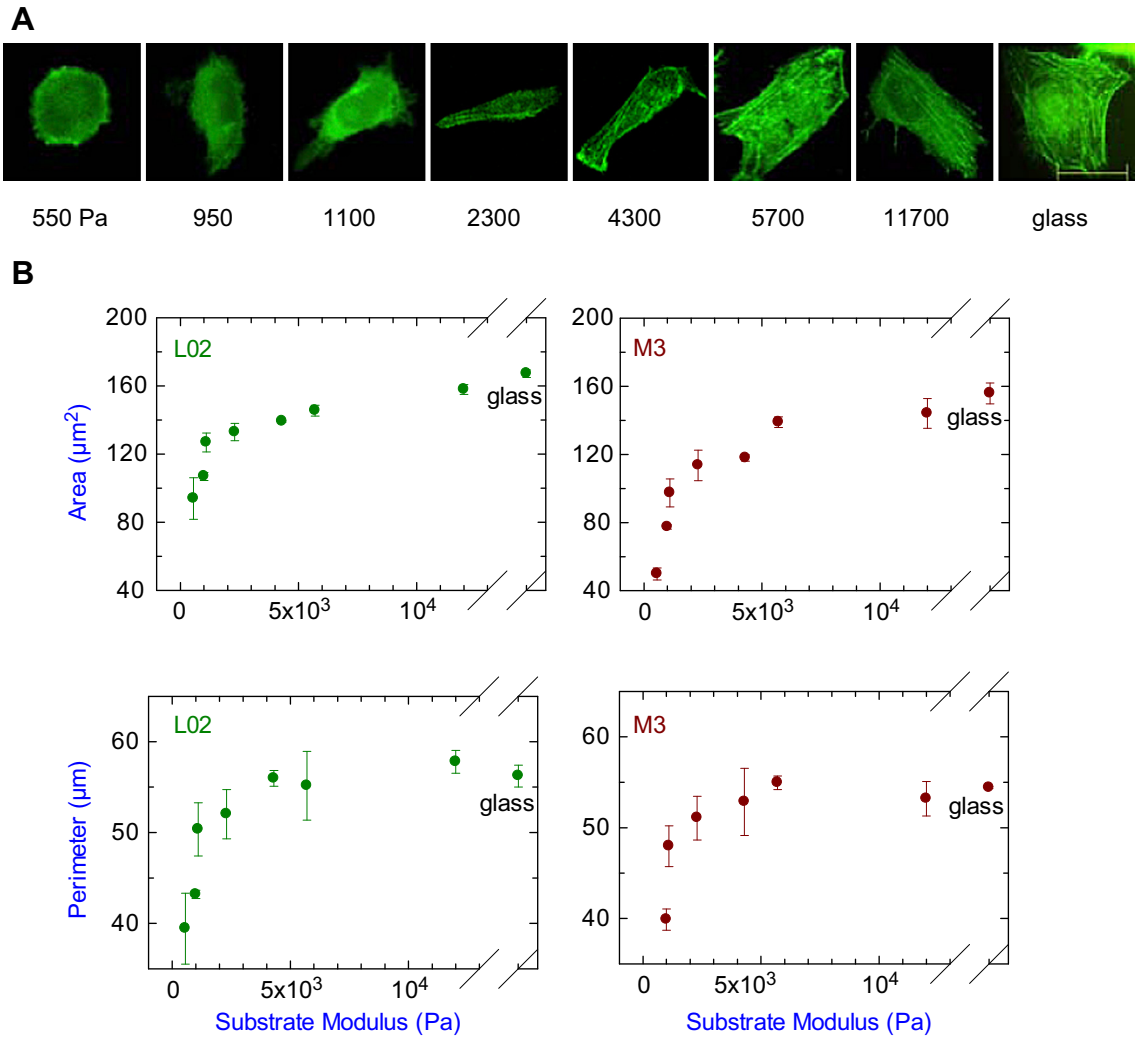

Fig. 2. Cell morphology as a function of substrate modulus. A, Typical microphotographs of cell morphology for M3 cells cultured for 10 h on substrates with different shear moduli. Scale = 15 μm. B, Dependency of spreading area and perimeter on substrate stiffness for L02 and M3 cells at steady state. The substrates were either polyacrylamide (PA) hydrogels of varying modulus or glass coverslips (modulus ~70 GPa). Fibronectin (2.5 μg/mL) was covalently cross linked to all substrate surfaces, and fibronectin uniformity was confirmed via immunofluorescence. Data points represent best fits of mean values of at least 30 cells at the steady state shown in Fig. 1B, and each error bar represents one standard deviation and serves as the estimate for standard uncertainty.

2. Materials and methods[3]

2.1. Preparation and mechanical properties of polyacrylamide gels

Polyacrylamide (PA) gels were prepared as described [16]. Gels with different stiffness values were achieved by varying the relative amounts of acrylamide and bis-acrylamide constituting the gel. Briefly, the PA gel solutions were prepared with acrylamide solution (A3553, Sigma, St. Louis, MO, USA) at final concentrations of 5.5%, 7.5%, and 12% by mass and bis-acrylamide (A2792, Sigma) at final concentrations from 0.06% to 0.3% by mass. To polymerize the solutions, 40 μL tetramethylethylenediamine (TEMED) and 40 μL of 10% ammonium persulfate (by mass, A3678, Sigma) were added with the appropriate amount of water to yield a final volume of 5 mL. The resulting solution was placed between two parallel glass sheets spaced 0.75 mm apart. After polymerization, the PA gel sheets were cut into cylindrical pieces with diameters of 15 mm or 25 mm.

The shear modulus (μ^s) of each PA gel was quantified by rheometry (TA instruments, AR2000ex). Prior to measurement, gels with a diameter of 25 mm were immersed in phosphate buffered saline (PBS) for 24 h to fully swell with water. μ^s was determined from the shear stress in phase with oscillatory frequency of 0.2 Hz and maximum shear strain (amplitude) of 1% at 37 °C. For each PA gel concentration, 3 to 5 samples were measured. The elastic modulus (E) of each gel was calculated assuming that all PA gels tested are incompressible and have a Poisson's ratio of 0.5, *i.e.*, $E = 3^*\mu^s$. No significant difference in shear modulus was found for PA gels with and without fibronectin coatings.

2.2. Cross-linking and analysis of adhesion proteins

A heterobifunctional crosslinker, sulfo-SANPAH (*N*-sulfosuccinimidyl-6-(4′-azido-2′-nitrophenylamino) hexanoate, Pierce 22589, Rockford, IL, USA), was used to crosslink human plasma fibronectin (F0895, Sigma) onto the PA gel surfaces. First, the top surface of the gel was completely covered with 1 mmol/L sulfo-SANPAH solution and irradiated for 10 min using an ultraviolet (UV) lamp. This entire process (coating-irradiation) was repeated once. Excess crosslinker was removed via three washes of 3 mL 200 mmol/L HEPES (H3375, Sigma) at pH 8.6. Afterwards, 200 μL of fibronectin solution (2.5 μg/mL, 25 μg/mL, or 100 μg/mL in HEPES) was added to the PA gel and reacted for 12 h at 4 °C. Fibronectin-coated PA gels were washed twice with Roswell Park Memorial Institute (RPMI)-1640 medium to remove unreacted fibronectin prior to cell seeding. For fibronectin visualization, fibronectin-coated PA gels were incubated with mouse anti-human plasma fibronectin primary antibody (1:200, F7387, Sigma) overnight, washed with PBS twice, and incubated with rhodamine-conjugated goat anti-mouse secondary antibody (R-6393, Invitrogen, Carlsbad, CA, USA) for 1 h. After staining, samples were imaged

[3] Certain commercial materials, equipment, and software are identified in this paper in order to specify adequately the experimental and analysis procedures. In no case does such identification imply recommendation or endorsement by the National Institute of Standards and Technology (NIST) nor does it imply that they are necessarily the best available for the purpose.

using a laser scanning confocal microscope (Leica, Germany) equipped with a 100× objective lens, and immunofluorescence analyses were performed to exam fibronectin uniformity on the surfaces. Glass substrates were functionalized and characterized following the same procedures.

2.3. Cell culture and morphology

Human hepatic cell line (L02) and human hepatocellular carcinoma cell line with highly metastatic potential (HCCLM3, termed M3) were obtained from the Liver Cancer Research Institute of Zhong Shan Hospital of Fudan University. L02 and M3 cells were routinely cultured in RPMI-1640 medium supplemented with 10% (by volume) fetal calf serum at 37 °C and 5% CO_2. PA gels (15 mm in diameter) and glass substrates were sterilized by immersing in 75% alcohol for 30 min, washing twice with HEPES for 30 min each, and then exposing to UV light for 30 min. Afterwards, PA gels and glass substrates were placed in individual wells of 12-well plates and seeded with 10^5 cells per well.

To capture the dynamic process of cell spreading on glass substrates, cells were imaged in 30 min intervals for 2 h and then in 2 h intervals for up to 10 h by inverted phase contrast microscopy. Cell perimeter and area of at least 30 cells were quantified at each time point using Image J software [26]. To quantify cell morphology at steady state as a function of substrate modulus, cells were cultured for 10 h, fixed with 4% paraformaldehyde, and stained for the actin cytoskeleton with 0.5 μg/mL fluorescein isothiocyanate (FITC)-phalloidin (Sigma). After washing with PBS, fixed cells were visualized on a Leica epifluorescence microscope with 100× oil immersion objective. Experiments were repeated at least three times, with at least 40 cells evaluated for each condition per repeat.

2.4. Atomic force microscopy

The stiffness of cells cultured for 10 h on PA gels and glass substrates coated with 2.5 μg/mL concentrated fibronectin was quantified using atomic force microscopy (AFM, JPK Instruments, NanoWizard II, Germany). Measurements were obtained at room temperature in tapping mode using quadratic pyramid cantilevers with a nominal stiffness of 0.04 N/m. The half-angle to face of the AFM tip was 17.5°, and the Poisson's ratio of the cell was taken to be 0.5, typical for soft biological materials [27]. Employing the AFM software, the tip was positioned precisely over the perinuclear region between the edge of the cell and the nucleus. Force-displacement curves were used to calculate the apparent cell stiffness (E) of individual cells ($N \geq 30$).

3. Results

3.1. Typical cell spreading

Fig. 1 provides typical development of cell area and perimeter for human normal (L02) and cancerous (M3) liver cells on glass substrates coated with fibronectin. When cells adhere to substrates, binding of diffusible cell membrane receptors to immobilized ligands on the substrate (*i.e.*, fibronectin) mediates adhesive interactions [28,29]. As binding events increase, cells spread and the cell-substrate adhesion zone grows. Within 10 h, these cells reach a steady state where cell area and perimeter have plateaued, and major changes in morphology associated with active development of cell spreading are complete. Throughout spreading, cellular traction is formed at cell-substrate adhesion sites, and substrate deformation is induced. As substrate modulus changes, traction, and therefore the final cell morphology, is expected to vary. Fig. 2 demonstrates experimentally that substrate modulus alters steady state cell area and perimeter.

3.2. Hypothesis and mathematical model of total free energy

The key mechanism by which substrate stiffness influences cell morphology is the energy tradeoff between the stabilizing influence of the cell-substrate interfacial adhesive energy and the destabilizing influence of the total elastic strain energies in the system. A continuum model is used to prove our hypothesis that stability of a given cell morphology depends upon total free energy (E_{tot}) of the system, and further to show that morphological response to substrate modulus can be used to estimate intrinsic cell modulus. The adaptation of a continuum description for the energy in the cell and substrate is appropriate because the actin mesh-size

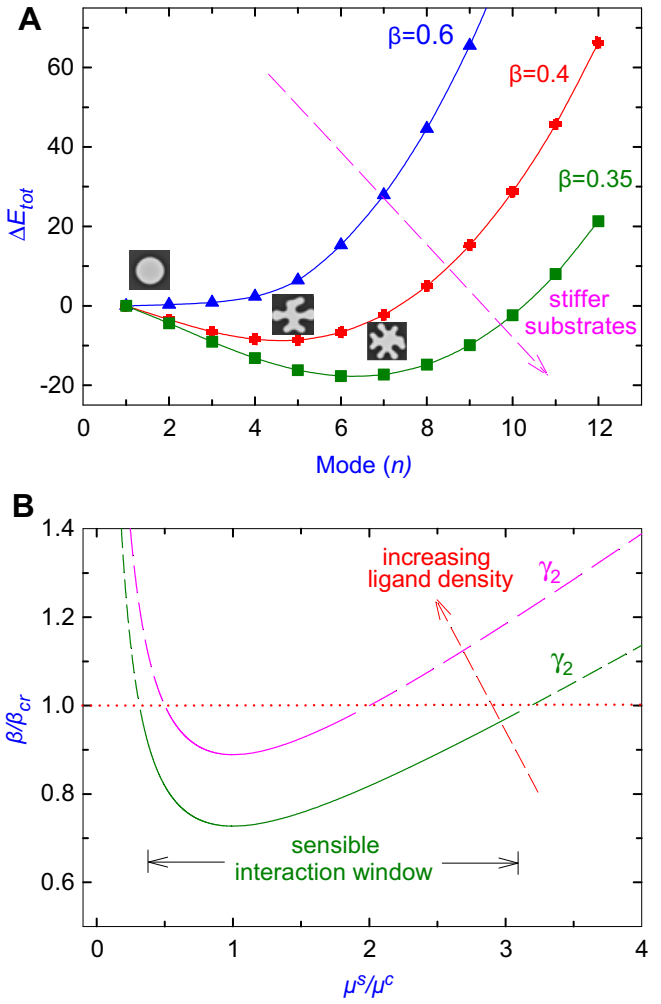

Fig. 3. Theoretical determination of morphological stability due to substrate stiffness. A, The energy variation (ΔE_{tot}) as a function of perturbation mode n for different values of β that reflect changes in substrate rigidity while cell rigidity and interfacial energy density are kept constant. The morphological perturbation can be described mathematically as $r(\theta) = R_o + \sum_n \delta_n \exp(in\,\theta)$, where R_o and r are the radii of the cell at the initial state and perturbed states, respectively, θ is the angular coordinate, n is a positive integer denoting the discrete azimuthal wave number, i is the imaginary unit, and δ_n represents the perturbation amplitude of the nth mode. β, the ratio of interfacial energy density to strain energy density of the cell/substrate system, is defined as $\beta = \mu^s\gamma/(1-\nu^s)\tau^2$, μ^s and ν^s are the shear modulus and Poisson's ratio of the substrate, respectively. γ is the interfacial energy density along the cell edge, and τ is the traction of the adherent cell. It should be noted that the morphologies in the insets are for illustration purposes only. Experimental results are not expected to mirror the regular patterns seen here. B, The variation of β/β_{cr} as a function of substrate to cell rigidity ratio, μ^s/μ^c, for two interfacial energies, $\gamma_1$and γ_2 ($\gamma_2 > \gamma_1$), corresponding to two different cell/substrate systems. The *sensible* interaction window is defined as a window of substrate/cell rigidity ratio in which cells can sense and respond to the change in substrate modulus.

(<0.1 μm) and observed minimal cell shape size (periphery) are orders-of-magnitude different [30].

When steady state morphology is achieved, *i.e.*, when active cell spreading (Fig. 1A) is completed, E_{tot} in the cell/substrate system is the sum of the interfacial energy or work of adhesion (E_{int}), the strain energies in the cell (E^c_{str}) and substrate (E^s_{str}), and other energies (E_{oth}, *e.g.*, surface energies of the cell and substrate):

$$E_{tot} = E_{int} + E^c_{str} + E^s_{str} + E_{oth} \quad (1)$$

E_{int} is due to biochemical reaction energy at cell-substrate binding sites and is primarily stored in a narrow strip along the

cell periphery at focal adhesions [31,32]. and are attributed to elastic responses in the cell and substrate, respectively, due to traction generated along stress fibers through actin-myosin contraction and transmitted to the substrate across integrin linkages. Changes in substrate stiffness alter the cell-substrate force balance. The subsequent force-based feedback control loop alters the focal adhesions and cell morphology. Consequently, cell morphology is characterized by competition between E_{int} and E_{str} ($E_{str} = E^c_{str} + E^s_{str}$), with E_{int} stabilizing the morphology and E_{str} destabilizing it. The cell morphology is energetically favorable when E_{tot} is minimized. If E_{tot} is not minimized, cell morphology may change, *e.g.,* through the reorganization of focal adhesions, so as to reduce the energy in the system. Therefore, the energetic favorableness of cell morphology at steady state is governed by the variation of E_{tot} (ΔE_{tot}) in the cell/substrate system associated with any cell shape perturbation, which can be expressed as:

$$\Delta E_{tot} = E^p_{tot} - E^u_{tot} \quad (2)$$

where superscripts p and u represent perturbed and unperturbed states, respectively.

ΔE_{tot} was calculated based on this biophysics to determine cell morphology stability at steady state. For problem tractability and mathematical simplicity (feasible calculations), a number of idealizations were made. A hypothetical adherent cell at steady state is assumed to have a circular spread morphology and isotropic traction. The cell and substrate are assumed to be an elastic membrane and structure, respectively. A homogenous interfacial energy density exists and is assumed to be uniformly distributed along the cell periphery. The cell then receives a small morphological perturbation along its edges that can be described mathematically as a discrete azimuthal wave number, n (perturbation mode). Cell area and volume remain unchanged during perturbation. With these simplifications, we believe our approach still captures the main features of the substrate rigidity effect on the cell/substrate system.

The dependency of cell morphology on the minimization of E_{tot} is elucidated using the relationship between ΔE_{tot} and n (Supplementary Data) for various substrate moduli at a constant interfacial energy density (γ) and cell modulus (Fig. 3A). The variation in substrate modulus is reflected by β, the ratio of interfacial energy density to strain energy density. When β is large (*e.g.,* $\beta = 0.60$), ΔE_{tot} is always positive and attains a minimum at (circular morphology), and any perturbation is *energetically unfavorable*. Thus, for our hypothetical cell, the initial circular morphology is preferred. Lower β, indicative of increasing strain energy density due to stiffer substrates, shifts the ΔE_{tot}–n curve below zero. For example, when $\beta = 0.35$, ΔE_{tot} is negative for most perturbation modes considered and $n \approx 7$ is the most energetically favorable morphology. Decreases in β can therefore give rise to morphological instabilities of the initial circular state. Since cell area is assumed constant, greater morphological instability due to a lower β can only be compensated by an increased cell periphery to increase the interfacial energy and stabilize the cell. This phenomenon will be demonstrated later via a measured morphological index (cell roundness). Thus, our model shows that a cell will select an appropriate morphology as a function of β, presumably through assembly/disassembly of focal adhesions.

Both the substrate modulus relative to the cell modulus and the interfacial energy (*i.e.,* fibronectin density) also alter cell morphological stability. Fig. 3B gives the variation in β versus the substrate to cell shear modulus ratio (μ^s/μ^c) for different interfacial energy densities, and. β is normalized by a critical value β_{cr}, determined by setting $\Delta E_{tot} \equiv 0$. For a given initial cell morphology, perturbation mode, and cell/substrate system, a β_{cr} exists such that $\Delta E_{tot} = 0$. When $\beta \geq \beta_{cr}$, interfacial energy dominates ΔE_{tot}, ΔE_{tot} is positive, and cell morphology is unchanged (stable) from the initial circular morphology as substrate modulus varies. When $\beta < \beta_{cr}$, strain energy dominates, ΔE_{tot} is negative, and the initial morphology becomes unstable.

The relations between β and μ^s/μ^c (Fig. 3B) are of particular significance in the interaction window, defined as the region where $\beta < \beta_{cr}$. In this region, the substrate modulus is comparable to the cell modulus, and β reaches a minimum. Accordingly, morphological changes due to variations in substrate modulus occur only when cell and substrate moduli are comparable, such that a *sensible* interaction can occur (*i.e.,* maximum mechanical interaction). The interaction window contains two modes of behavior. When $\mu^s/\mu^c < 1$, β decreases with increasing substrate stiffness as approaches 1, and the energetically-favorable morphology mode, n, increases (Fig. 3A). As μ^s/μ^c further increases above 1 in the interaction window, β increases and n decreases (cell is more rounded). The results explain the cell morphological response to substrate modulus by revealing that relative rigidity between cell and substrate is more critical than absolute substrate rigidity.

The extent of mechanical interactions between the cell and substrate, indicated by the width of the interaction window, is narrowed and up-shifted with the increase of γ (Fig. 3B), suggesting lower n values at steady state for higherγ. Once γ surpasses a threshold, the interaction window disappears. Below the threshold, a range of γ values enable the cell to sense and respond to substrate modulus. Experimentally for a given cell, this optimal γ range corresponds to a concentration range of adhesive ligands (*e.g.,* extracellular matrix (ECM) proteins such as fibronectin) on the substrate.

The minimization of ΔE_{tot} provides the basis for estimating cell modulus. The change in the trend of morphological stability (inflection point in Fig. 3B) corresponds to if an interaction window exists ($\beta < \beta_{cr}$). Therefore, cell modulus can be estimated as substrate modulus at this inflection. In the mathematical model, the cell is assumed to have a uniform modulus. For simplicity, we do not consider separately the cell membrane, cortex and cytoskeleton: cell modulus determined by observing the inflection point is an aggregate quantity. More importantly, the model is based on the competition of energies, reflecting the knowledge that cells change shape by assembling/disassembling cytoskeletal networks to relieve strain and stress. Therefore, the modulus represents an intrinsic (suspended) cell modulus, independent of cytoskeleton reorganization during the processes of shape development and change. The intrinsic nature of the observed cell modulus, which is independent of ligand concentration, is supported by the unchanging inflection point as a function of γ (Fig. 3B).

3.3. Experimental validation and application

Our concept of total free energy and our method to measure cell modulus using cell morphology analysis were validated using experiments that quantified steady state cell morphology as a function of substrate modulus and fibronectin concentration. Results confirm a biphasic cell response to substrate modulus and a dependency of the interaction window on fibronectin concentration. The experiments further provide the intrinsic cell moduli of normal and cancerous liver cells.

Roundness, S ($=C^2/4\,\pi\,A$, effectively equivalent to n in Fig. 3A), is selected as the morphological index to represent alterations in cell shape. Cell perimeter (C) and projected spreading area (A) at steady state are associated with interfacial energy and strain energy, respectively, and vary with substrate modulus (Fig. 2). $S = 1$ represents a circular spread area, and higher values indicate increased deviation from circularity. For substrates coated with 2.5 μg/mL fibronectin, the morphological index of both cell types has a

biphasic development as substrate modulus increases (Fig. 4), matching the biphasic modeling results (Fig. 3B). As Fig. 2B demonstrates, other cell morphology metrics such as cell perimeter and area do not represent the biphasic morphology response to substrate modulus.

Two additional fibronectin concentrations and the same variation in substrate modulus demonstrated the effects of cell/substrate adhesion on the interaction window. With 25 μg/mL fibronectin, the upper bound of the interaction window is reduced from 20 kPa (for 2.5 μg/mL fibronectin) to 5 kPa (Fig. 4), confirming the predicted loss of sensitivity to substrate modulus at higher ligand densities (γ in Fig. 3B). As fibronectin is further increased to 100 μg/mL, no alterations in roundness are observed. These results further support predictions of Fig. 3B that cell morphology is unchanged with respect to substrate modulus when interfacial energy passes a threshold. This threshold is system dependent and is expected to vary with parameters such as cell type, growth medium, and ligand. When fibronectin exceeds the threshold, many cell receptors are arrested firmly during cell attachment, and fewer receptors are mobile to implement morphological changes. The enhanced cell-substrate interactions increase the interfacial energy and prevent the cell from changing its morphology.

Following our theoretical results, at the morphological inflection point. Thus, cell shear moduli based on observed inflections in

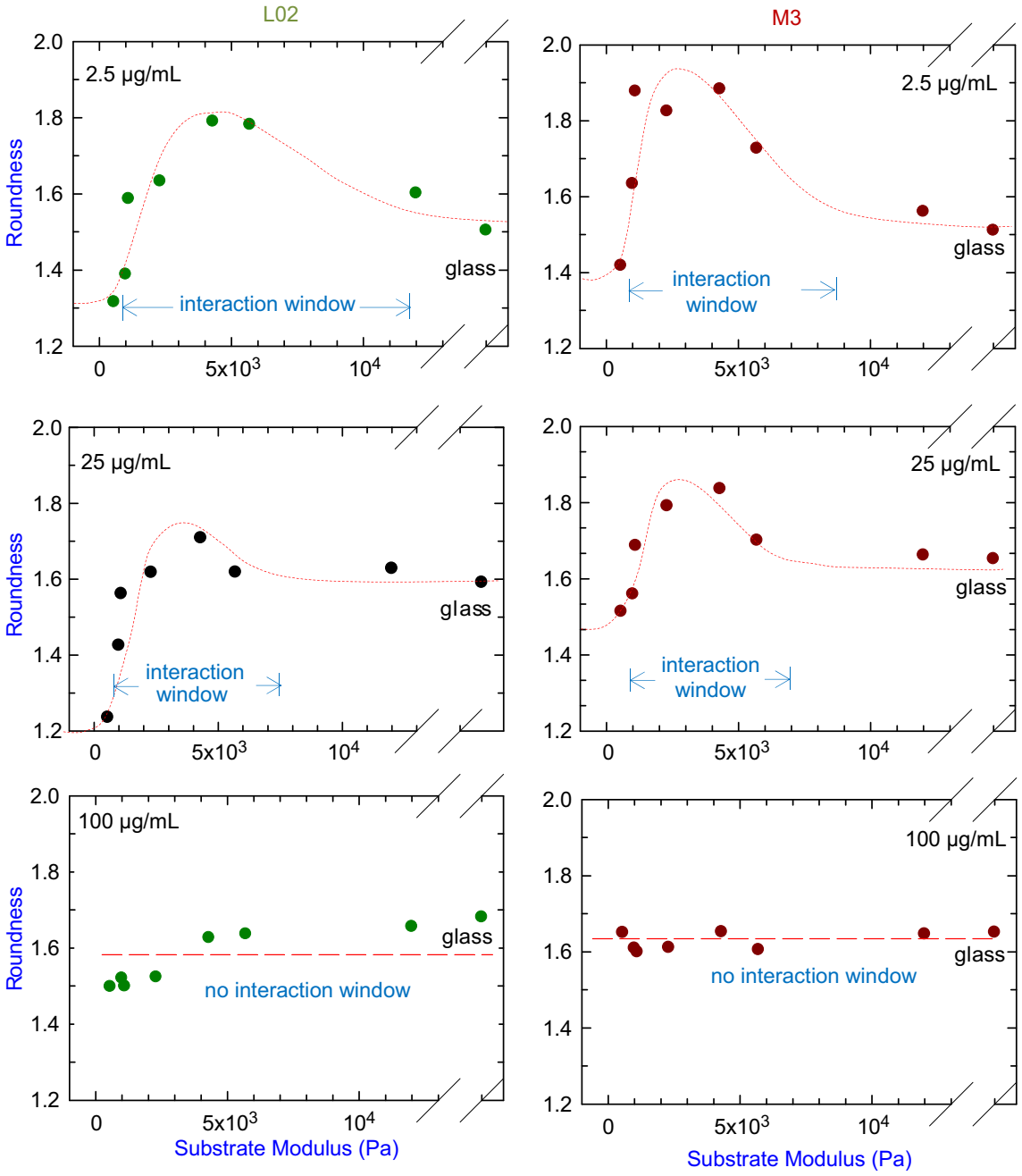

Fig. 4. Morphology index of cell roundness (S) as a function of substrate modulus. L02 and M3 cells were analyzed after 10 h of culture on substrates with varying moduli coated using 2.5 μg/mL, 25 μg/mL, or 100 μg/mL fibronectin. Each data point is obtained using mean values for area and circumference (*i.e.*, values for 2.5 μg/mL fibronectin data are taken from Fig. 2B). Dashed lines indicate best fit curves. For 2.5 μg/mL and 25 μg/mL, the roundness approaches an asymptote as substrate stiffness increases, as expected, since cell traction increases with increasing substrate stiffness and reaches a maximum due to biochemical limits [33–36].

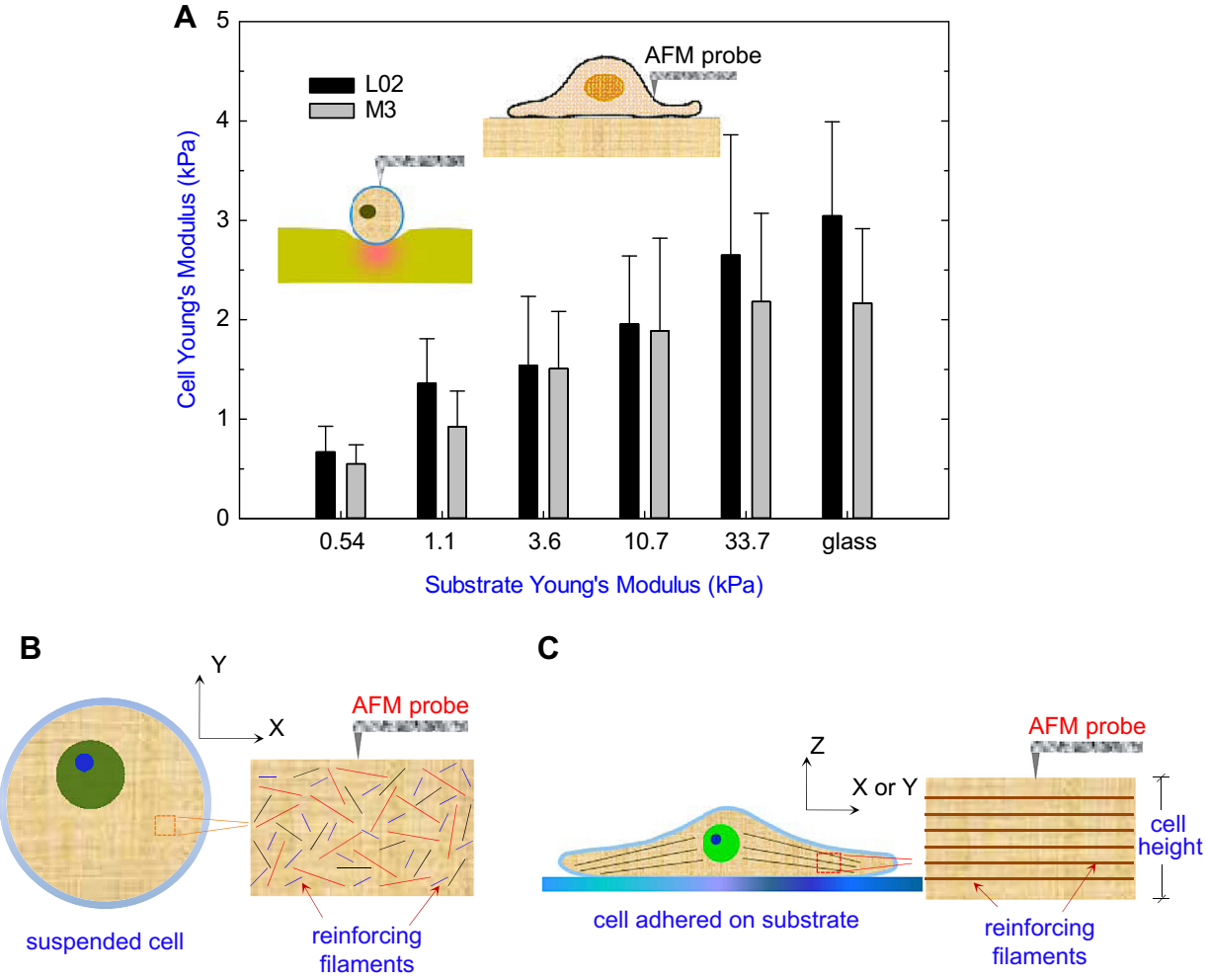

Fig. 5. Measurement of cell elastic modulus using AFM. A, Elastic modulus of adherent cells on substrates with different elastic moduli, as measured by AFM. The modulus is probed over the central region of the cell (to the side of the nucleus) and within a certain indentation limit. Data points are the mean value from 3 measurements of each of at least 30 cells, and each error bar represents one standard deviation and serves as the estimate for standard uncertainty. B, Schematic of a suspended cell having randomly oriented short filaments and isotropic properties. C, Schematic of an adherent cell having continuous, oriented reinforcing filaments and anisotropic properties. The AFM tip probes in the transverse direction and therefore does not detect mechanical properties associated with the longitudinally-oriented fibers in the spread cell.

roundness are ≈3.6 kPa for L02 cells and ≈2.8 kPa for M3 cells. Reduced intrinsic stiffness of metastatic cancer cells relative to normal cells agrees with studies of apparent cell stiffness [11]. In addition, the sensible interaction window size of M3 cells is reduced relative to L02 cells, perhaps indicating stronger cell-substrate interactions (similar to increasing γ in Fig. 3B). Increased interactions with the substrate may be due to alterations in expression patterns of fibronectin-binding integrins, which change in liver cancer cells relative to normal cells [37]. The predicted cell moduli do not change with fibronectin concentration (2.5 μg/mL and 25 μg/mL fibronectin), just as changes in γ do not alter the inflection point in Fig. 3B.

3.4. Comparison to AFM methods

Most cell modulus measurements emphasize relative changes in cell stiffness (using methods that are ECM and/or cytoskeleton dependent) or an "apparent stiffness" rather than intrinsic moduli (14). AFM-measured Young's moduli (E) of L02 and M3 cells on substrates with different rigidities were (1–3) kPa (Fig. 5A), lower than intrinsic cell moduli derived from morphology analysis (Fig. 4), which provided E for L02 and M3 cells of 10.8 kPa and 8.4 kPa, respectively, assuming incompressible cells ($E \approx 3 \times \mu^c$). These differences can be explained by considering the cytoskeleton of suspended and adherent cells. Cells can be treated as composites consisting of matrix components (*e.g.*, cytoplasm) and reinforcing fibers (mainly filaments of different types and lengths) [38,39]. Suspended cells can be considered to have randomly oriented short filaments [24] and isotropic properties (Fig. 5B). Cells spread on two-dimensional substrates have polymerized cytoskeletal networks and can be rationalized as cells enhanced with continuous filaments mostly parallel to the substrate (Fig. 5C). Spread cells will thus have anisotropic properties dependent on the orientation of reinforcing filaments (longitudinal and transverse directions). From this analogy, cell moduli obtained using AFM have greater contributions from transverse moduli (perpendicular to reinforcing filaments). Reinforcing fibers in adherent cells (Fig. 5C) do not contribute significantly to stiffness in the transverse direction unless the fiber volume fraction is very high, so AFM-measured moduli of adherent cells are expected to be lower than moduli of suspended cells.

One may argue that a cell adherent on a soft substrate (*e.g.*, elastic modulus of 1.1 kPa) has a very limited spread area (Fig. 2A: rounded cell on substrate with = 550 Pa) and should therefore have

a cytoskeletal organization similar to a suspended cell. Yet, AFM-measured cell moduli on substrates with $E = 0.54$ kPa and 1.1 kPa ($\mu^s = 180$ Pa and 367 Pa) are lower than cell moduli obtained using morphology analysis, and very similar to the substrate moduli. In these cases, we believe that the cells are much stiffer than the substrates, such that the substrates and not the cells deform during AFM measurements (inset, Fig. 5A), making cells appear softer than they are. Other AFM studies also measured a cell modulus equivalent to the substrate modulus at very low substrate moduli (14). This concept is further supported by cells on $E = 3.6$ kPa ($\mu^s = 1200$ Pa) substrates, which have AFM-measured cell moduli comparable to neither the substrate modulus nor the cell moduli determined by morphology analysis. These cells are well spread (Fig. 2A, $\mu^s = 1100$ Pa) with an area and perimeter significantly greater than cells at $\mu^s = 550$ Pa (Fig. 2B) and are not expected to indent into the substrate to skew the measurement. Since those spread cells have a developed, anisotropic cytoskeleton, AFM measurements provide an apparent modulus lower than that determined by morphology analysis, as described above.

4. Discussion

Our argument on the *sensible* interaction window can help interpret varying observations of cell response to substrate modulus, where cells require different substrate moduli for normal function and differentiation [18,21,25,40–44]. Fibroblasts are fan-shaped on stiffer substrates and more rounded on compliant substrates (μ^s<1 kPa) [21]. These observations concur with our model predictions (Fig. 3B), which demonstrate that when μ^c (~2 kPa, based on the morphological transition in their data) is comparable to μ^s and $\mu^s/\mu^c \leq 1$, cell morphology becomes less rounded with increasing substrate rigidity. Cells become more rounded when $\mu^c >> \mu^s$, equivalent to fibroblasts on substrates with very low stiffness ($\mu^s < 1$ kPa) [21]. In contrast, neurons on substrates with μ^s ranging from 50 Pa to 550 Pa extend more branches on softer substrates and have no preference for branching on stiffer ones [19,20]. Based on our model and a reported shear modulus of bovine spinal cord of ≈50 Pa [19], it can be inferred that μ^c of a neuron is ≈50 Pa. This inference can be rationalized using results in Fig. 3B: when μ^c is comparable to μ^s and $\mu^s/\mu^c \geq 1$, cell morphology becomes less rounded (more branches) with *decreasing* substrate rigidity (softer). Thus, the interaction window location depends upon cell type, and cell modulus can be estimated by morphology analysis.

Moreover, our model can explain conflicting literature results regarding effects of substrate modulus on cell morphology. For example, one study revealed that substrate modulus had minimal effects on neutrophil circumference [21], whereas another study showed significant changes in neutrophil area with substrate modulus using the same substrate [45]. When evaluating these seemingly inconsistent results using our model, the role of adhesive ligands becomes apparent. The first study used 140 μg/mL fibronectin [21], which likely increased cell-substrate interfacial energy and prohibited an interaction window. The second study used 10 μg/mL fibronectin [45], which allowed for sensible interactions and changes in cell morphology. These findings highlight both the utility of the model in interpreting data and the importance of ligands in these studies. However, we note that these and many other papers report either cell area or cell perimeter, rather than a more comprehensive morphological indicator, such as roundness, to correlate cell morphology and function. Unlike area and perimeter, roundness reflects the energy interchange associated with morphological changes described by the cell-substrate interactions presented in this study. Thus, there exists a body of images that, if re-analyzed for additional morphology parameters, would provide substantial information on intrinsic cell moduli without additional experimentation.

5. Conclusions

The cell response to biochemical and/or mechanical stimuli is extremely diverse and complex, thus measurements of cell modulus without perturbation are very desirable. Our breakthrough in measuring intrinsic cell modulus is based on and validated by theory, experiments, and existing literature that demonstrate that morphology of adherent cells can be rationalized by the minimization of total free energy in the cell/substrate system. Live cells are self-regulating systems that can select their own response to a given external perturbation or internal force. Our work indicates that this response, though biological in nature, follows the laws of the energy interchange in order to achieve the self-regulated behavior. This knowledge can be extended to yield implications for thermodynamics studies into a cell's innate self-regulating activity and new thoughts regarding energetic processes at the subcellular level.

Acknowledgments

This work was supported in part (Y.Y., J.L.Z, and L.Y.) by grants from National Nature Science Foundation of China (11032012, 30870608 and 10472137), Innovation and Attracting Talents Program for College and University ('111' Project) (B06023), Key Science and Technology Program of CQ CSTC (CSTC, 2009AA5045) and sharing fund of Chongqing University's large-scale equipment.

Appendix A. Supplementary data

Supplementary data related to this article can be found at http://dx.doi.org/10.1016/j.biomaterials.2013.09.014.

References

[1] Chen CS, Mrksich M, Huang S, Whitesides GM, Ingber DE. Geometric control of cell life and death. Science 1997;276:1425–8.
[2] Fletcher DA, Mullins RD. Cell mechanics and the cytoskeleton. Nature 2010;463:485–92.
[3] Dulinska I, Targosz M, Strojny W, Lekka M, Czuba P, Balwierz W, et al. Stiffness of normal and pathological erythrocytes studied by means of atomic force microscopy. J Biochem Biophys Methods 2006;66:1–11.
[4] Ochalek T, Nordt FJ, Tullberg K, Burger MM. Correlation between cell deformability and metastatic potential in B16-F1 melanoma cell variants. Cancer Res 1988;48:5124–8.
[5] Li QS, Lee GYH, Ong CN, Lim CT. AFM indentation study of breast cancer cells. Biochem Biophys Res Commun 2008;374:609–13.
[6] Evans ND, Minelli C, Gentleman E, LaPointe V, Patankar SN, Kallivretaki M, et al. Substrate stiffness affects early differentiation events in embryonic stem cells. Eur Cell Mater 2009;18:1–14.
[7] Pillarisetti A, Desai JP, Ladjal H, Schiffmacher A, Ferreira A, Keefer CL. Mechanical phenotyping of mouse embryonic stem cells: increase in stiffness with differentiation. Cell Reprogram 2011;13:371–80.
[8] Qiu H, Zhu Y, Sun Z, Trzeciakowski JP, Gansner M, Depre C, et al. Short communication: vascular smooth muscle cell stiffness as a mechanism for increased aortic stiffness with aging. Circ Res 2010;107:615–9.
[9] Lu YB, Iandiev I, Hollborn M, Körber N, Ulbricht E, Hirrlinger PG, et al. Reactive glial cells: increased stiffness correlates with increased intermediate filament expression. FASEB J 2011;25:624–31.
[10] Swaminathan V, Mythreye K, O'Brien ET, Berchuck A, Blobe GC, Superfine R. Mechanical stiffness grades metastatic potential in patient tumor cells and in cancer cell lines. Cancer Res 2011;71:5075–80.
[11] Cross SE, Jin YS, Rao J, Gimzewski JK. Nanomechanical analysis of cells from cancer patients. Nat Nanotechnol 2007;2:780–3.
[12] Place ES, Evans ND, Stevens MM. Complexity in biomaterials for tissue engineering. Nature Mater 2009;8:457–70.
[13] Tee SY, Fu J, Chen CS, Janmey PA. Cell shape and substrate rigidity both regulate cell stiffness. Biophys J 2011;100:L25–7.
[14] Solon J, Levental I, Sengupta K, Georges PC, Janmey PA. Fibroblast adaptation and stiffness matching to soft elastic substrates. Biophys J 2007;93:4453–61.
[15] Lekka M, Laidler P. Applicability of AFM in cancer detection. Nat Nanotechnology 2009;4:72–3.
[16] Beningo KA, Lo CM, Wang YL. Flexible polyacrylamide substrata for the analysis of mechanical interactions at cell-substratum adhesions. Methods Cell Biol 2002;69:325–39.

[17] Discher DE, Janmey PA, Wang YL. Tissue cells feel and respond to the stiffness of their substrate. Science 2005;310:1139–43.
[18] Engler AJ, Sen S, Sweeney HL, Discher DE. Matrix elasticity directs stem cell lineage specification. Cell 2006;126:677–89.
[19] Flanagan LA, Ju YE, Marg B, Osterfield M, Janmey PA. Neurite branching on deformable substrates. Neuroreport 2002;13:2411–5.
[20] Georges PC, Miller WJ, Meaney DF, Sawyer ES, Janmey PA. Matrices with compliance comparable to that of brain tissue select neuronal over glial growth in mixed cortical cultures. Biophys J 2006;90:3012–8.
[21] Yeung T, Georges PC, Flanagan LA, Marg B, Ortiz M, Funaki M, et al. Effects of substrate stiffness on cell morphology, cytoskeletal structure, and adhesion. Cell Motil Cytoskeleton 2005;60:24–34.
[22] Saha K, Keung AJ, Irwin EF, Li Y, Little L, Schaffer DV, et al. Substrate modulus directs neural stem cell behavior. Biophys J 2008;95:4426–38.
[23] Paluch E, Heisenberg CP. Biology and physics of cell shape changes in development. Curr Biol 2009;19:R790–9.
[24] Zemel A, Rehfeldt F, Brown AEX, Discher DE, Safran SA. Optimal matrix rigidity for stress fiber polarization in stem cells. Nat Phys 2010;6:468–73.
[25] Pelham RJ, Wang YL. Cell locomotion and focal adhesions are regulated by substrate flexibility. PNAS 1997;94:13661–5.
[26] Abramoff MD, Magelhaes PJ, Ram SJ. Image processing with ImageJ. Biophotonics Int 2004;11:36–42.
[27] Touhami A, Nysten B, Dufrene YF. Nanoscale mapping of the elasticity of microbial cells by atomic force microscopy. Langmuir 2003;19:4539–43.
[28] Giancotti FG, Ruoslahti E. Integrin signaling. Science 1999;285:1028–32.
[29] Katsumi A, Orr AW, Tzima E, Schwartz MA. Integrins in mechanotransduction. J Biol Chem 2004;279:12001–4.
[30] Ni Y, Chiang MYM. Cell morphology and migration linked to substrate mechanics. Soft Matter 2007;3:1285–92.
[31] Katoh K, Kano Y, Noda Y. Rho-associated kinase-dependent contraction of stress fibers and the organization of focal adhesions. J R Soc Interface 2011;8:305–11.
[32] Bickel T, Bruinsma R. Focal adhesion: physics of a biological mechano-sensor. Biophys J 2003;83:3079.
[33] Wang N, Naruse K, Stamenović D, Fredberg JJ, Mijailovich SM, Tolić-Nµrrelykke IM, et al. Mechanical behavior in living cells consistent with the tensegrity model. PNAS 2001;98:7765–70.
[34] Wang N, Tolić-Nµrrelykke IM, Chen J, Mijailovich SM, Butler JP, Fredberg JJ, et al. Cell prestress. I. Stiffness and prestress are closely associated in adherent contractile cells. Am J Physiol Cell Physiol 2002;282:C606–16.
[35] Zemel A, Bischofs IB, Safran SA. Active elasticity of gels with contractile cells. Phys Rev Lett 2006;97:128103.
[36] Deshpande VS, McMeeking RM, Evans AG. A bio-chemo-mechanical model for cell contractility. PNAS 2006;103:14015–20.
[37] Wu Y, Qiao X, Qiao S, Yu L. Targeting integrins in hepatocellular carcinoma. Expert Opin Ther Targets 2011;15:421–37.
[38] Ingber DE. Tensegrity I. Cell structure and hierarchical systems biology. J Cell Sci 2003;116:1157–73.
[39] Ingber DE. Tensegrity II. How structural networks influence cellular information processing networks. J Cell Sci 2003;116:1397–408.
[40] Engler AJ, Griffin MA, Sen S, Bönnemann CG, Sweeney HL, Discher DE. Myotubes differentiate optimally on substrates with tissue-like stiffness: pathological implications for soft or stiff microenvironments. J Cell Biol 2004;166:877–87.
[41] Peyton SR, Putnam AJ. Extracellular matrix rigidity governs smooth muscle cell motility in a biphasic fashion. J Cell Physiol 2005;204:198–209.
[42] Jiang G, Huang AH, Cai YF, Tanase M, Sheetz MP. Rigidity sensing at the leading edge through $\alpha v\beta^3$ integrins and RPTPα alpha. Biophys J 2006;90:1804–9.
[43] Guo WH, Frey MT, Burnham NA, Wang YL. Substrate rigidity regulates the formation and maintenance of tissues. Biophys J 2006;90:2213–20.
[44] Ingber DE. Mechanical control of tissue morphogenesis during embryological development. Int J Dev Biol 2006;50:255–66.
[45] Oakes PW, Patel DC, Morin NA, Zitterbart DP, Fabry B, Reichner JS, et al. Neutrophil morphology and migration are affected by substrate elasticity. Blood 2009;114:1387–95.